ELSEVIER

European Journal of Radiology 24 (1997) 20–32

EUROPEAN JOURNAL OF RADIOLOGY

Mammographic image analysis

R.P. Highnam*, J.M. Brady, B.J. Shepstone

Engineering Science, Departments of Radiology and Engineering, Parks Road, Oxford University, OX1 3PJ Oxford, UK

Received 5 September 1996; accepted 5 September 1996

THEME

Abstract

We describe our recent progress aimed at computer analysis of mammograms. The overall aim is to provide the clinician with reliable quantitative information. We summarise a representation we have developed of the 'interesting' (non-adipose) tissue in a breast, then put the representation to work in three ways: (i) to propose a new quantitative measure to aid in diagnosing masses; (ii) to explore the possibility of reducing by half the radiation dose required for a mammogram; and (iii) recalling some of the results that can be provided by differential compression mammography, in which mammograms are taken at two slightly different compressions. Copyright © 1997 Elsevier Science Ireland Ltd.

Keywords: Mammography; Quantitative computer analysis; Dose reduction

1. Introduction

This paper describes some of our recent progress in computer processing of (X-ray) mammograms. Section 2 describes the physics-based model that is the background to our work. In Section 3, we introduce a novel quantitative feature to aid in the diagnosis of masses by examining the tissue that surrounds the mass. In Section 4 we show how image enhancement of a mammogram taken without an anti-scatter grid can yield an image of high visual quality and information content yet with half the radiation dose to the patient. Finally, in Section 5, we illustrate the value of taking two mammograms at slightly different compressions, a technique we have called 'differential compression mammography' [1,2]. Because differential compression requires that two mammograms be taken of the same breast, to become clinically acceptable, almost certainly this will necessitate a dosage reduction technique like that in Section 4.

This paper builds on the analysis presented in [3] to which the interested reader is referred for a technical presentation of the underlying mathematics. Here, the main ideas are summarised in the following sections by way of example images. The overall aim of our work can be stated succinctly: to provide the clinician with reliable quantitative information. For a clinician to use an image processing system routinely, he must understand what it claims to do and he must have confidence in the results it produces. As a step towards this we have developed a system 'Xmammo' whose interface uses only terms familiar to the clinician: move the automatic exposure control (AEC), reduce the exposure time, change the film gradient, etc. Fig. 1 shows a typical screen shot of Xmammo. In addition we have developed a tutorial system to help radiographers and radiologists learn about mammography through using Xmammo; experimental evaluation of the efficacy of the tutorial material is highly encouraging. The key issue, however, is the reliability of the image processing and the resulting confidence of the clinician.

Reliability is a major problem because, as an application of image processing, mammographic images pose a tough challenge because they have poor signal-to-noise

* Corresponding author. Tel.: +44 1865 282184; fax: +44 1865 273908; e-mail: rph@robots.ox.ac.uk

PII S0720-048X(96)01110-2

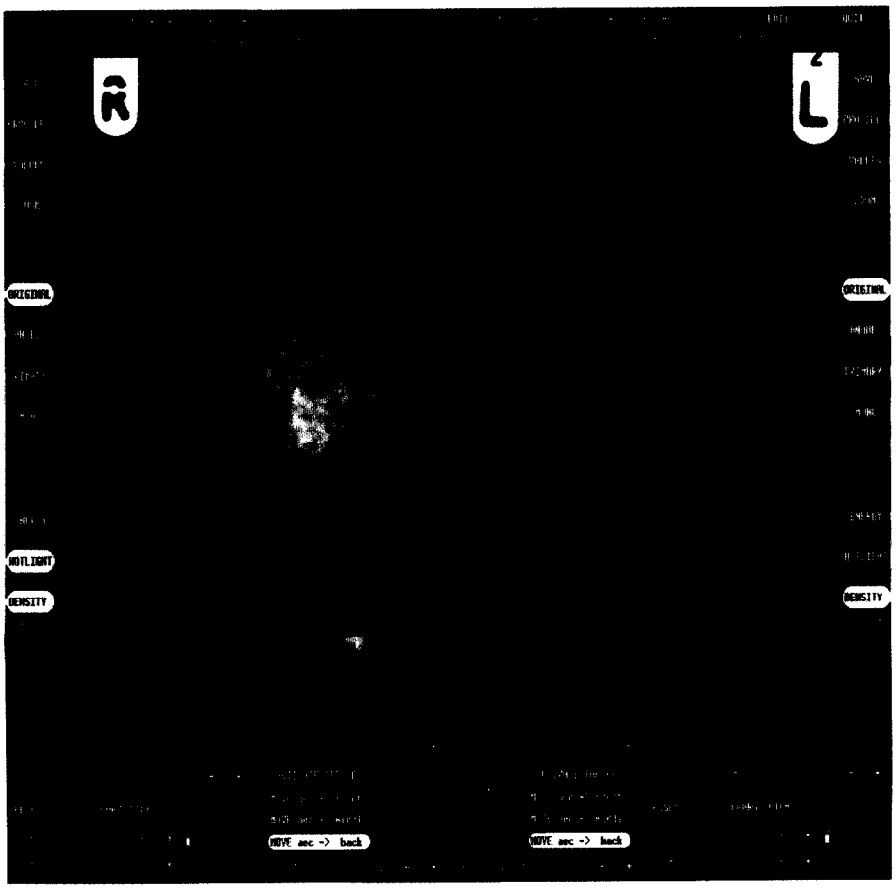

Fig. 1. 'Xmammo' is a model-based image enhancement software package. All the image processing operations are presented in terms familiar to the clinician so that he/she can understand and therefore trust the processing. The use of model-based techniques is less likely to introduce artifacts or remove important indicators. In this example the operator is using the hotlight option to view the breast edge.

ratio. This is largely because the images exhibit complex textures, resulting from scattered photon radiation [4] and because there is inevitably a compromise between radiation dose and image quality. Worse, abnormalities appear as quite subtle, irregular, often non-local differences in intensity. Moreover, the images are inevitably cluttered due to superimposition, the background varies greatly between different breasts, and there is relatively weak control of the imaging acquisition. Unfortunately, while there have been many papers written on the application of image processing to mammography, the vast majority of work has been of limited scope and incorporates only general non-mammography specific image processing considerations. The dangers are obvious: image smoothing may make lesions easier to locate, but can remove calcifications and spiculations; edge sharpening may appear to improve an image from the image processor's perspective but can transform a malignant lesion into one that appears to a radiologist to be benign. Generally, reported techniques for digitally filtering mammographic images have been replete with mathematics but are based on physically dubious assumptions and give poor results. Fortunately, however, there is a growing number of more soundly based techniques that have been tested thoroughly and that give good results [5–9].

Our approach is based on the belief that in order to be reliable and predictable, medical image processing must be based on a model of how the image is formed [1,3,4,10]. In the case of mammography, this means we must model the way that X-rays pass through breast tissue, are absorbed, and scattered before exposing the film. Central to our approach is a two-dimensional representation that we call h_{int} and which is summarised in the next section. The value of h_{int} at the pixel location (x, y) represents the amount of non-fat ('interesting') tissue between the pixel and the X-ray source. Crucially, h_{int} provides for image normalisation by separating out the particular imaging conditions (e.g., film speed, exposure time, tube characteristics) from the intensity changes due to tissue variation, which is what is really important to diagnosis. Normalisation is a vital prerequisite to statistical analysis of populations of patients [3]. Unfortunately, up to now, almost every application to mammography of pattern recognition, not least using neural networks, has failed to first normalise the data in a suitable manner.

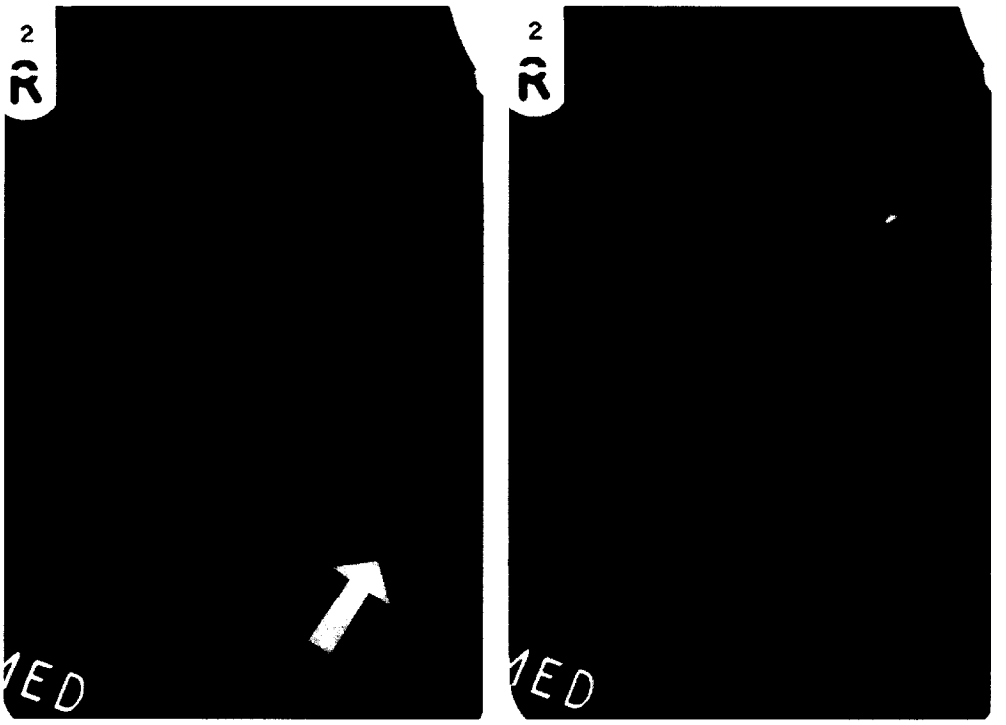

Fig. 2. On the left is an original cranio-caudal mammogram of a 54 year old woman. There is a benign circumscribed mass near the chest wall. On the right is an enhanced version of original. In this example, the image has been enhanced by the software removal of the effects of scattered radiation and then simulation of a monoenergetic examination (18 keV).

2. The h_{int} representation

Ideally, one might hope for a quantitative three-dimensional representation of the breast with each voxel labeled with a tissue type, such as: glandular, fibrous, cancerous, fat, calcium. Given the X-ray attenuation within a voxel it is certainly possible to classify fat since it has relatively low linear attenuation coefficients. It is also possible to classify likely occurrence of calcium, which is practically radio-opaque. However, the remaining breast tissues are those that comprise anatomically significant events in breast disease, such as cysts, malignant masses, fibroadenomas, and they are difficult to resolve from X-ray attenuation measurements alone. These observations led us to classify breast tissue into one of three types: 'interesting tissue', fat and calcium. For our work, we consider calcium to have been detected [5] so that there are basically only two tissue classes to consider, and we use the thicknesses of interesting tissue (h_{int} cm) and fat (h_{fat} cm) as our quantitative breast measurements. Note that we have no 3D information about where the interesting tissue is in respect to the fat.

If the breast thickness H is known then $H = h_{int} + h_{fat}$. A result of our previously reported scatter removal algorithm [4] was to demonstrate that it is possible to estimate h_{int} and h_{fat}. This means that we can convert an image into a representation which effectively assumes that the fat has risen to float on top of the interesting tissue surface, then peels off the fat leaving a representation $h_{int}(x, y)$. This concept, while obviously approximate, suffices for a surprising number of purposes. Informally, this representation can be viewed as a surface and clinically significant effects such as masses appear as features on this surface, e.g., small hills. Note that this is fundamentally different from regarding the original mammogram as a surface, since the h_{int} representation is a quantitative measure of anatomical tissue in vertical pencils of the breast.

If $D(x, y)$ is the original X-ray density image, the image enhancements we develop for the Xmammo system can be represented by:

$$D_{given}(x, y) \rightarrow h_{int}(x, y) \rightarrow D_{enhanced}(x, y)$$

The first step is to construct the corresponding interesting tissue surface representation $h_{int}(x, y)$, thereby removing the particular imaging conditions (e.g., exposure time) and normalising the data. The second step corresponds to choosing imaging conditions (e.g., a different exposure time). In a similar way, the first step can consist of estimating the scattered radiation that appears to defocus the image; in that case the second step amounts to displaying it with the scatter removed. Fig. 2 shows an original mammogram and the mammogram that would have been obtained had there been no scatter. Fig. (3) shows the h_{int} representation for the image in the form of a 3D surface.

Other applications require that we modify the h_{int} surface, that is, modify the estimated interesting tissue in the breast. Such applications can be represented by:

$$D_{\text{given}}(x, y) \rightarrow h_{\text{int}}(x, y) \rightarrow h_{\text{int}}(x, y) \rightarrow D_{\text{simulated}}(x, y),$$

Here the modification takes place in the second step. As an example, we show how one can simulate the appearance of masses of various types in various contexts. There are many reasons for doing this including developing a teaching tool for radiologists and aiding radiologists with picturing the mass in 3D. [3] shows an example of our simulation.

We conclude this section by noting that an estimate of the breast thickness H, that is to say the separation between the compression plates, is critical to the estimate of h_{int}. We have shown in [3] that it is in fact possible to estimate H from h_{int}, by constraining the shape and appearance of the breast edge. Other techniques have proved to be cumbersome [11], so it would be better to find the thickness from the breast image itself. This is important because knowledge of the breast thickness also allows an estimate of the radiation dose during the examination. Although we can estimate H from h_{int} it is encouraging that manufacturers are including automatic recording of plate separation in newer machines and we urge imaging protocols that record all information relevant to how an image is formed. More generally, we note that calibration data is critical to the estimation of h_{int}; [3] gives details.

3. A quantitative feature for image analysis

As a typical application of the h_{int} representation, we consider the development of a quantitative feature to aid in the diagnosis of circumscribed masses. About one in three of the circumscribed masses that go to open surgical biopsy turn out to be benign. This is a far lower ratio than is usual in mammography, and reflects the use of ultra-sound and FNA as immediate follow-ups when a circumscribed mass is seen on film. In order to further improve the ratio, and to reduce the psychological trauma of recalled women, we explore the use of image analysis to provide objective, quantitative descriptions of circumscribed masses that can be used to aid diagnosis. In general our approach is to look at perceived wisdom in radiology and then to try and give a physical explanation for this wisdom, for example:

- why do 'malignant masses tend to be denser than their surround'?
- what is the 'halo-of-safety'?
- why do benign masses tend to have sharper edges than malignant ones?

Once we have established a valid physical explanation in terms of h_{int} (which is the most suitable representation for this) it is relatively easy to implement. It could be said that we are using quantitative image processing to try and define more precisely what radiologists are looking for.

We have set out, initially, to try and quantify the statement: malignant masses tend to be denser than their surroundings. To obtain such a quantitative description requires not only that the images are normalized, but also that the effects of tissues that are being superimposed onto the mass image are also removed. In order to estimate the tissue being superimposed on a mass we studied the area surrounding the mass on the basis that the tissue projected there would be similar to the tissue above and below the mass. For example, if we found that most of the tissue surrounding a mass in an image was fat then it would seem reasonable to conjecture that tissue above and below the mass was also fat. We note however that there are well-known phenomena which suggest that the tissue surrounding a mass is not independent of the mass. These phenomena include increased vascularity, and the so-called 'halo-of-safety' which is said to exist around some benign lesions. Angiogenesis appears to be an accepted phenomenon and is the reason for the interest in using MRI to view rate of uptake of gadolinium. However, the 'halo-of-safety' is more controversial with some radiologists describing it as 'compressed fat' [12], whilst others consider it simply to be a visual phenomenon [13]. Swann et al. [14], in what appears to be the most comprehensive study to date, investigated the halo sign and concluded that it is not a guaranteed indicator of a benign process, indeed they noted its presence around at least 25 malignant lesions that they had seen.

Since it appears that we must be careful about what surrounding area we should use to try and estimate what is above and below a mass we decided initially to investigate using h_{int} surface curvatures to determine whether the tissue surrounding a mass is representative of the tissue above and below the mass. We found that there appears to be a measurable 'cover' around every mass, irrespective of whether it is benign or malignant (see Fig. 3). Quantifying the extent of this cover and comparing between the two screening views—cranio-caudal and medio-lateral oblique—reveals that variation in the extent might be a guide to malignancy (the idea of comparing the two views comes from our work on differential compression which is outlined later).

We start by describing the database of circumscribed masses that we use. We then consider the h_{int} images generated from that database as 3D surfaces and study the principal surface curvatures within and around the mass. We then look at the change of these curvatures and compare the results between the views.

THEME

Fig. 3. This shows the h_{int} representation viewed as a surface. Near the chest wall there is a circumscribed mass. Note the dipping of the surface around the edge of the mass. In the h_{int} representation the heights at each pixel have physical meaning.

3.1. Database

One of the most notable aspects of all previous work on mammographic image analysis is the failure of algorithms to perform equally well between different databases. The work we outline in this section has worked identically on a number of different calibrated image databases collected over the last 5 years. In all our databases we store with each image details of X-ray tube voltage, time of exposure, breast thickness etc. With this calibration data we are able to transform the original mammographic images to the h_{int} representation. Our database consists of four smaller databases, the first three of which were generated at Oxford. The first database (oxDCM) was generated in 1991 using a Joyce-Loeble scanning microdensitometer and contains mammograms taken at different breast compressions (see Section 5 below). The second (oxGRID) was generated in 1995 using a Lumisys scanner and contains mammograms taken with and without an anti-scatter grid (see Section 4). The third (oxDATA) was also generated using a Lumisys scanner and contains images from a sample assessment clinic. Finally, the fourth (nwDATA) was generated using a Lumisys scanner and contains mammograms of women who attended a hospital in Newark, USA. The films in the database were kindly digitized for us by the Royal Marsden Hospital and Philips Laboratories, Briarcliff. The images used in the work reported here have a pixel resolution of 300 microns, but this is entirely for efficiency of processing. Applying the techniques to 50 μm resolution images is straightforward.

In the database we have some 20 examples of circumscribed masses depicted in cranio-caudal and medio-lateral oblique views. However, we are only sure of the diagnosis for 14 of the masses. For this current work, we assume prior manual segmentation of the masses in the two views.

3.2. Surface curvature within and around a mass

We can picture a circumscribed mass as a hill in the h_{int} representation. Fig. 4 shows an example of a profile across a malignant mass and a benign mass. Mathematically, moving with a constant heading along the h_{int} surface from a point on the mass to a point in the surrounding area one might expect to first go downhill (as you leave the mass), then join the surrounding region that is relatively flat. A 'halo of safety' would correspond to first going downhill (off the mass) into a

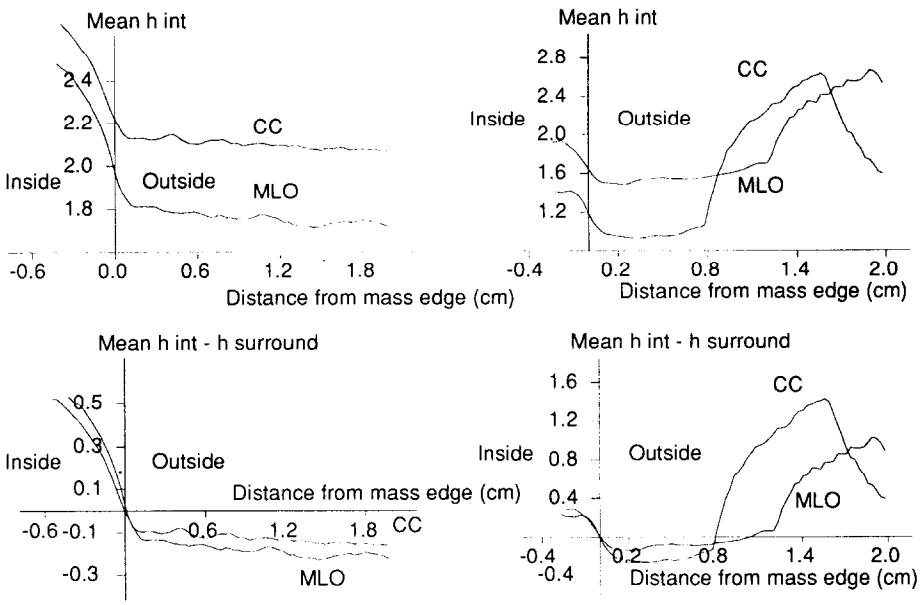

Fig. 4. The top graphs show the average h_{int} at a certain distance from the edge of the mass. The bottom graphs show the difference between h_{int} and an estimate of the surrounding tissue component. The surround is estimated here using a planar fit to the data—this removes any linear gradients in the surface. The graphs on the right are from a benign mass and there is a clear 'moat' around it. The graph on the left is a malignant mass imbeded in fat, again there is an area outside the mass that appears to be non-independent of the mass.

surrounding moat (the halo), then climbing uphill a little onto the surrounding region. Mathematically, this would correspond to a path portion of negative curvature surrounded by a moat of positive curvature.

Actually, the local differential geometry of surfaces is a little more complex. The following aims briefly to make the ideas intuitively obvious. The interested reader can be referred to any standard book on differential geometry for the details. Imagine slicing a surface with a planar blade so that the plane of the blade contains the local normal to the surface. Such a section is called a 'normal section'. Clearly, the blade can be rotated about an axis that corresponds to the surface normal, to give a family of normal sections of the surface, all at the same surface point and differing only in the orientation of the blade. The curvature of the curve resulting from the normal section in a given blade orientation is called a normal curvature. If the surface were a sphere, for example, all normal curvatures would be equal (in fact they would all be the inverse of the radius of the sphere). If the surface were a cylinder, the normal curvature would be zero for a slice where the blade was parallel to the axis, and would be equal to the inverse of the cylinder radius for a cross-section slice.

Generally, the normal curvature varies with direction of slice. The normal curvature attains two ex treme values (maximum and minimum) and these are in perpendicular directions, just like in the case of the cylinder. The curvature is a second differential of the curve. The sum of the maximum and minimum curvatures is proportional to the sum of the second differentials in two perpendicular directions. In fact, it can be shown that the sum of second differentials taken in two perpendicular directions (called the Laplacian of the surface) is independent of which particular directions are chosen. Since it is likely that one of the second differences will be small we can look at the sign of the average Laplacian over an area, and this aids numerical stability. It also circumnavigates the problem of overlaying tissues by effectively smoothing the image; an alternative approach would be to remove them using a model-based approach [15].

As part of an initial investigation, we computed the average Laplacian within the mass, and the average Laplacian in a 0.5 cm surround of the mass shape. The surround was defined by applying binary morphological dilation up to the required size. In every case (40 images), the mass had a negative average Laplacian and the surround had a positive average Laplacian (Table 1). These results are insensitive to the size of the kernel for computing the Laplacian. These results appear to indicate that genuine masses (both benign and malignant) exhibit a negative Laplacian, whilst the surrounding tissue always exhibits a positive Laplacian.

Whilst a change in sign of the Laplacian is expected, it is unlikely that such consistent results over a region could be attained unless there is a physical explanation. One plausible explanation is that there is some kind of 'cover' around every mass. Indeed, Fig. 4 seems to suggest this although other explanations are possible.

Table 1
The average Laplacian for our database of circumscribed masses

Image	Diagnosis	CC, Mean Laplacin		MLO, Mean Laplacian	
		Mass	Surround	Mass	Surround
oxDATA009L	Benign	−0.014	0.005	−0.021	0.003
oxDATA010L	Benign	−0.019	0.004	−0.011	0.001
oxDATA012R	Benign	−0.013	0.004	−0.012	0.003
nwDATA000L	Unknown	−0.018	0.004	−0.009	0.002
nwDATA001L	Unknown	−0.006	0.001		
nwDATA008L	Benign	−0.004	0.003	−0.005	0.001
nwDATA009La	Benign	−0.014	0.002	−0.013	0.002
nwDATA009Lb	Benign	−0.003	0.002	−0.001	0.001
nwDATA010L	Malignant	−0.005	0.003	−0.011	0.002
nwDATA013L	Unknown	−0.005	0.001	−0.003	0.001
nwDATA017L	Unknown	−0.014	0.003	−0.007	0.003
nwDATA019L	Unknown	−0.005	0.003	−0.002	0.001
oxDCM003L	Benign	−0.007	0.002	−0.013	0.002
oxDCM005L1	Benign	−0.007	0.005	−0.003	0.003
oxDCM005L2	Benign	−0.028	0.001		
oxDCM006L	Malignant	−0.025	0.003	−0.108	0.007
oxGRID003R	Benign	−0.005	0.005	−0.008	0.008
oxGRID006Ra	Malignant	−0.019	0.003	−0.017	0.005
oxGRID006Rb	Malignant	−0.011	0.003	−0.014	0.007

THEME

3.3. Extent of the cover

To further investigate the measured phenomena we used the change of sign of the average Laplacian to determine the extent of the cover around each mass. We took only those cases where the diagnosis was confirmed, and compared the extent of the cover in the two views. Table 2 shows the results for benign masses which cover a wide variety of background types. The results show a wide variance in cover extent between the views. Figs. 5 and 6 show examples of the covers found around benign masses.

Table 3 shows the cover extent for confirmed malignant masses. Again, there is wide variance in the background, but this time there is very little variation in the extent of the cover for the malignant masses in the two views. This is significant given that we are comparing images taken at two different views and are therefore dealing with changing compression, view, and geometry. Figs. 7 and 8 show examples of covers that were computed around malignant masses.

Table 2
The cover extents for benign circumscribed masses

Image	Cover extent (cm)		Variation (max−min/av)
	CC	MLO	
oxDATA009L	0.240	0.120	0.667
oxDATA010L	0.330	0.120	0.933
oxDATA012R	0.420	0.300	0.333
nwDATA008L	0.240	0.150	0.462
nwDATA009L	0.300	0.180	0.500
oxGRID003R	0.330	0.420	0.462
oxDCM003L1	0.120	0.300	0.857
oxDCM003L2	0.090	0.300	1.077
oxDCM005L1	0.120	0.270	0.769
oxDCM005L2	0.180	0.270	0.400

3.4. Discussion

There are several observations we can make about these results. The first is that the cover which we are measuring appears not to be related to the projected size of a mass, or mass type, and is not therefore related to the tissues being displaced by the mass as it grows. This comes from the fact that if the mass was a sphere (for example) and the cover was uniform around that sphere then:

$$V_{\text{mass}} = \frac{4}{3}\pi r^3_{\text{mass}}$$

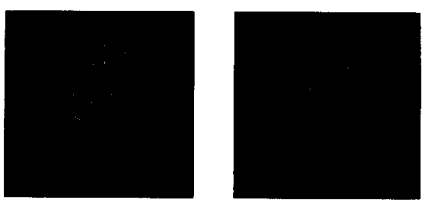

Fig. 5. This shows the cover extent found for a benign lesion (oxDATA010L) in the cranio-caudal (left) and medio-lateral oblique (right) views. The size of the extent changes markedly despite the mass area remaining almost constant.

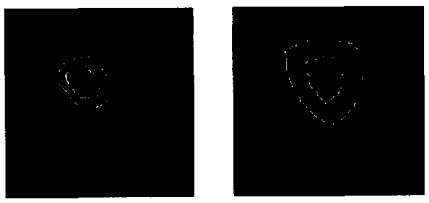

Fig. 6. This shows the cover extent found for a benign lesion (oxDCM003L) in the cranio-caudal (left) and medio-lateral oblique (right) views. The size of the extent changes markedly between views.

$$V_{\text{cover}} = \frac{4}{3}\pi r^3_{\text{cover}} - V_{\text{mass}}$$

And, if $V_{\text{mass}} = V_{\text{cover}}$ then $r_{\text{cover}} = 2^{1/3} r_{\text{mass}}$, where V is volume and r is the radius. A supporting observation here is that if the cover was displaced tissue then we would expect it to be invisible since one would expect the tissue being displaced to have roughly the same composition as the tissue into which it is being moved. In Fig. 3 the measured cover is apparent.

In fact, our results seem to indicate that the cover surrounds the mass, and probably is equal in thickness all-round. This cover appears to deform with the mass so that benign masses have widely varying cover extents, whereas solid masses have fixed extent (the change in cover extent is unlikely to be just from view since benign lesions are likely to be fairly symmetric). This in turn suggests that compression is having a large effect on the benign masses and so some measure of compressibility based upon the mass shape itself might well allow differentiation of benign and malignant masses. Of particular significance in Table 3 is that the area of the projected malignant masses for nwDATA010L almost doubles between the view, and yet the measured cover stays the same. This we could expect given that the mass is malignant and therefore less likely to be symmetric; it is also a result we would expect given our model of the cover as a equal thickness covering of the mass. The fact that malignant masses are less likely to be symmetric means that using the area of the projected mass is not a good discriminator since a change in mass area could be due to view or compression. The results indicate a solid cover for the malignant masses and this might be supported by LeBorgne's sign. The significance of compression can

Table 3
The cover extents for malignant circumscribed masses

Image	Halo extent (cm)		Variation (max−min/av)
	CC	MLO	
nwDATA007R	0.210	0.180	0.154
nwDATA010L	0.270	0.240	0.112
oxGRID006R0	0.150	0.180	0.182
oxGRID006R2	0.240	0.270	0.112

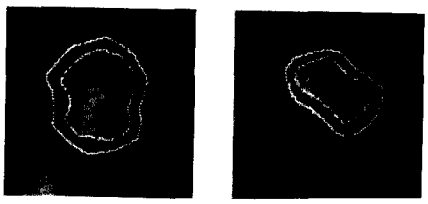

Fig. 7. This shows the cover extent found for a malignant lesion (nwDATA010L) in the cranio-caudal (left) and medio-lateral oblique (right) views. The size of the extent is almost identical despite the mass area almost doubling between the two views.

be seen in Table 2, where the cover extent varies slightly with compression (oxDCM003L, oxDCM005L) but not to the degree that would indicate great susceptibility (or numerical instability).

In our work to date, no attempt has been made to differentiate between benign lesions that are cysts, and benign lesions that are fibroadenomas. If the cover that is being measured is varying due to compression then one might expect fibroadenomas to give results similar to malignant masses. Similarly, it is possible to envisage a situation where the breast is not compressed firmly and a benign mass does not deform sufficiently for the covering to vary in extent.

There are other plausible explanations of the phenomena which we have outlined, including the possibility that what we are seeing has a different physical explanation for benign and malignant masses. A thorough clinical investigation of this feature is underway in the Breast Care Unit at the Churchill Hospital in Oxford. The investigation includes variation of the extent around the mass, and completeness of the extent.

4. Removing the anti-scatter grid

The use of an anti-scatter grid in mammography greatly improves image quality but necessitates an approximate doubling of the radiation dose and increased equipment cost. In this section, we investigate removing the effects of scatter from conventional mammograms by digitizing them and using image enhancement techniques rather than by an anti-scatter grid. As we noted

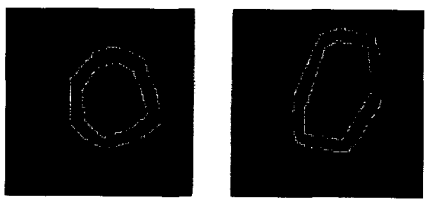

Fig. 8. This shows the cover extent found for a malignant lesion (oxGRID006R) in the cranio-caudal (left) and medio-lateral oblique (right) views. The size of the extent is almost identical despite the mass area varying.

THEME

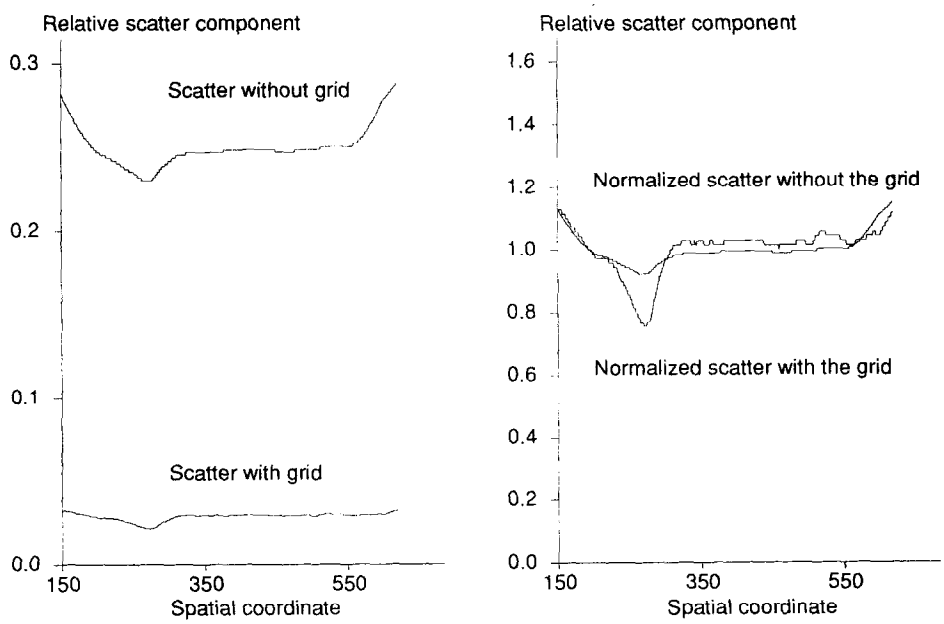

Fig. 9. The figure on the left shows the relative scatter component along a profile across an actual image for the case when a grid is used and when not. The scatter without the grid is clearly massive compared to the scatter with the grid. However, when the grid is used the scatter component is more reliant on the local tissue and so is of a higher frequency. This can be seen by dividing the two curves by their average. This is shown on the right.

earlier, our algorithm for scatter removal [4] enables us to be quite certain that no artifacts are created nor are important signs removed. Another major benefit is that the use of such a model allows an enhanced image to be generated in a clearly-defined manner: there is no need to experimentally refine thresholds, mask sizes, or contrast measures for each image. We begin this section with a basic theoretical analysis of the signal with and without the grid, and then show some practical results.

4.1. Theory

To perform a theoretical analysis we make some simplifying assumptions. The first is that we ignore extra-focal radiation since it is minimal for most of the breast area of the film. The second is that the grid doubles the time of exposure (experimental results confirm this). The third is that the primary signal passing through the same tissue but without the grid, and at the same time of exposure as with the grid, increases by 4/3; this is based upon the primary transmission rate of the Philip's grid at 18 keV [16]. The final assumption is that the scatter component for the same block of tissue without the grid, but at the same time of exposure as with the grid, increases by a factor of 5.0 [17].

The primary signal contains explicit information about the breast tissue, and so it is of considerable interest to compare the strength of the primary signal with and without the anti-scatter grid. The primary increases without the grid when the same time of exposure is used but since the time of exposure decreases we actually see a decrease in real terms. On the other-hand, scatter increases:

$$E_{\mathrm{p}}^{\text{no grid}}(x, y, t_{\mathrm{s}}^{\text{no grid}}) \approx \frac{2}{3} E_{\mathrm{p}}^{\text{grid}}(x, y, t_{\mathrm{s}}^{\text{grid}})$$

$$E_{\mathrm{s}}^{\text{no grid}}(x, y, t_{\mathrm{s}}^{\text{no grid}}) \approx \frac{5}{2} E_{\mathrm{s}}^{\text{grid}}(x, y, t_{\mathrm{s}}^{\text{grid}})$$

If one considers the signal-to-noise ratio in a mammogram in a classical manner then it appears that performing a mammogram without an anti-scatter grid and then digitally enhancing is doomed to failure. Take as the signal-to-noise ratio (SNR), the ratio of primary radiation to scattered radiation then, from the previous equation:

$$SNR^{\text{no grid}} = \frac{E_{\mathrm{p}}^{\text{no grid}}}{E_{\mathrm{s}}^{\text{no grid}}} \approx 0.267 \times SNR^{\text{grid}}$$

However, this analysis hides the fact that the noise, in this case scatter, is far more constant when the grid is not used and is therefore easier to model and remove. The important factor in our work is how much information there is in the image, and the noise that is important is not scatter but film noise and digitization noise [5]. Fig. 9 shows a profile across the scatter component computed using our model of scatter for the case with and without a grid.

If we assume that $E_{\mathrm{p}}^{\text{grid}}(x, y, t_{\mathrm{s}}^{\text{grid}})$ is the 'gold standard' and examine how we expect the image to appear

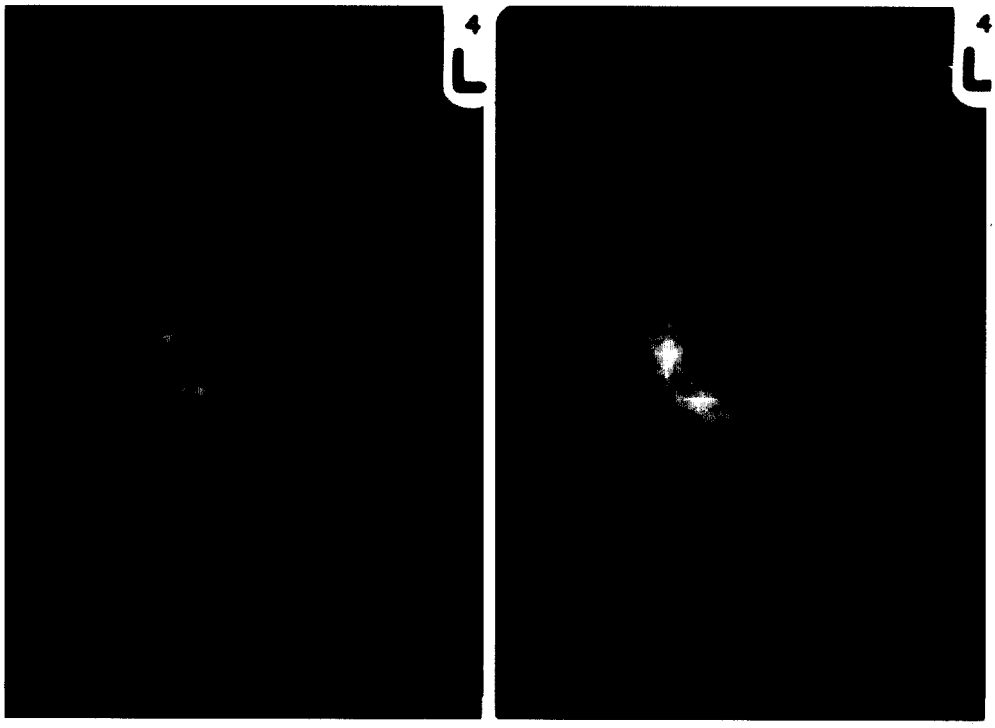

Fig. 10. On the left is a mammogram taken without the anti-scatter grid, and then digitally enhanced. On the right is a mammogram of the same breast taken with an anti-scatter grid.

without the grid when the same primary is attained. We can obtain the same primary by only reducing the time of exposure by 3/4 from that of when the grid is used. Assuming a linear film-screen curve and taking a gradient of 3.0 and an average scatter-to-primary ratio with the grid as 0.1, we can show that the film density without the grid rises by 0.291. This analysis predicts that to get the same primary without the anti-scatter grid as with it, we can reduce the time of exposure and hence radiation dose by 25% but the film will become markedly darker. This might mean that the film becomes too dark for visual inspection. Other work investigates the imaging of calcifications when a grid is not used [18].

4.2. Practical results and discussion

Fig. 10 shows an example of the images captured when a grid is used, and when it is not used and the image digitally enhanced. Clearly, there is a great deal of information in the non-grid image even though it initially looks very poor to the naked eye. Future work will address what is an acceptable reduction in the primary component and examine more closely the signal in the presence of calcifications. We note that the medical community still has to be convinced that the digitization process produces images of a high enough quality compared to the films produced by conventional mammography. However, the work here and the scatter model is equally applicable to directly-digital systems.

5. Differential compression mammography

Despite the many techniques available to the radiologist some 70–80% of open surgical biopsies reveal benign disease [19] and some 8–25% of cancers are 'missed' [20,21]. Whilst external physical examination of the breast can give some information about the physical properties of the breast tissue close to the breast surface, more reliable information about the deeper tissues and internal breast structures would aid more accurate diagnoses.

We proposed a novel way of obtaining information about these internal properties, by comparing mammograms taken with the breast compressed at different thicknesses [1]. For example, a mammogram might be taken with the breast compressed to a thickness of 5 cm, followed by a second mammogram with the breast compressed to a thickness of 6 cm. The movement and deformation which is seen by comparing these two mammograms is linked to the physical properties of the breast: mammographic signs which do not change position between the two mammograms might be fixed in some manner (e.g., by spicules to the chest wall); mammographic signs which appear not to change might represent a solid tissue structure (e.g., a malignant

Fig. 11. These show cranio-caudal view mammograms of the same breast under different compressions. On the left the breast is compressed to 6.5 cm. and on the right the breast is compressed to 6 cm. In this example there is a spiculated mass which displays relatively little movement compared to the tissue that is positioned next to it.

tumour). We dubbed this technique 'differential compression mammography'. A convenient way to view the movement and deformation is to digitize the films and to view them rapidly as a two-frame movie (the CD-Rom that accompanies [3] shows one such movie).

Our interest in breast compression arose from our attempts to automate the diagnostic procedure. Automated diagnosis must be robust to changes in the imaging conditions (as indicated earlier), and to changes in compression. We hope that the data provided by this study will enable us to make automated diagnosis robust to compression. The initial study that we carried out presented some interesting results, but due to the need for two films and hence double the radiation dose we did not do a larger trial. However, with the work outlined in the section above it appears that digital mammography offers the opportunity to reduce the radiation dose so that two films can be carried out safely.

5.1. Example results

Fig. 11 shows two cranio-caudal images of the same breast under different compressions. There is a spiculated mass in the breast. With increased compression the mass does not shift position whilst tissue around it moves appreciably and deforms. Fig. 12 shows another two cranio-caudal images of a breast under different compressions. These images are interesting not only because of the changes due to compression but also because of the difference in brightness between the two images due to the changing imaging conditions (i.e., time of exposure). These two mammograms show that as the breast is compressed blood vessels disappear. Since blood vessels going into a breast is a sign of increased chance of malignancy it might be prudent in certain cases to not compress the breast so far. This case illustrates one of the problems with mammography: there are many effects confounded together. In this case just because there appears to be no vessels going into the mass does not mean that the mass is not malignant, it means that either there are actually no vessels going into the mass or that the breast has been firmly compressed. Further examples of differential compression mammography can be found in [10].

6. Summary

Digital image processing of mammographic images has the potential to be of great benefit to the radiologist. However, simplistic or general purpose image processing which is not based on a physical model of the breast and X-ray process is unlikely to be of any use. In

Fig. 12. These show cranio-caudal view mammograms of the same breast under different compressions. On the left the breast is compressed to 6.5 cm, and on the right the breast is compressed to 5.5 cm. In this example the blood vessels evident under less compression have practically disappeared in the right mammogram. If increased vascularity is an indicator of cancer it might be better to image the breast under less compression than normal so that vessels going into masses can be visualised on the mammogram.

this paper we have reported on three aspects of our work which are based around models. In each case the work has had significant feedback to the imaging process itself. We note, in passing, that newer imaging techniques such as changing the tube voltage during exposure, or varying the exposure over breast, inevitably make quantitative analysis even harder. From the standpoint of reliable quantitative measurement based on image analysis it would be better to regard imaging as a way of optimally storing information (on film or in a computer) with visualisation and enhancement carried out subsequently.

The desire to obtain quantitative data from mammographic images is useful since it encourages imaging protocols and serious consideration of what breast disease is, how it develops and how it appears in a mammogram. In particular, since there are so many confounding effects in mammography such as the imaging conditions, view and compression we have been forced to either separate these confounding effects or to at least understand their separate contributions to the eventual image.

Our future work along these lines will investigate other quantitative features, such as compressibility, with a view to combining the results from several features to provide accurate diagnosis. Such analysis will include dealing with X-ray geometry and more than one view. We hope to develop a diagnosis system which could be used in a system geared towards augmenting and complementing the radiologist rather than replacing him/her (or even providing a second opinion).

Acknowledgements

The authors thanks the staff at the Breast Care Unit in the Churchill Hospital, Oxford, for their continuing support and encouragement. Particular thanks to Yvonne Swainston and Donald Peach. RPH thanks Philips Laboratories for support during his 9 month stay there and Chuck Carman and Gail Elliot for many useful discussions; JMB thanks the Epidaure Team at INRIA Sophia Antipolis, and Nicholas Ayache in particular, for tremendous support during his sabbatical there.

References

[1] Highnam RP, Shepstone BJ, Brady JM. Mammograms at different compression plate widths for the detection of breast cancer. In: Radiology and Oncology 91, Work in Progress. British Institute of Radiology 1991: 3.

[2] Highnam RP, Brady JM, Shepstone BJ. Differential compression mammography. Br J Radiol 1996; 69: 373–374.
[3] Highnam RP, Brady JM, Shepstone BJ. A representation for mammographic image processing. Med Image Anal 1996; 1: 1–19.
[4] Highnam RP, Brady JM, Shepstone BJ. Computing the scatter component of mammographic images. IEEE Med Imaging, 1994 13: 301–313.
[5] Karssemeijer N. Adaptive noise equalization and recognition of microcalcification clusters in mammograms. Int J Pattern Recognition Artificial Intelligence, 1993; 7: 1357–1376.
[6] Lefebvre F, Benali H, Gilles R, Kahn E, Dipaola R. A fractal approach to the segmentation of microcalcifications in digital mammograms. Med Phys 1995; 22: 381–390.
[7] Cerneaz NJ, Brady JM. Finding curvilinear structures in mammograms. In: Ayache N, ed. Lecture Notes in Computer Science, Nice, France, April 1995. Berlin: Springer 1995: 372–382.
[8] Miller L, Ramsey N. The detection of ill-defined masses by non-linear multiscale analysis. In: Nishikawa R, ed. 3rd International Workshop on Digital Mammography. Amsterdam: Elsevier 1996.
[9] Parr TC, Astley SM, Taylor CJ, Boggis CR. Model-based classification of linear structures in digital mammograms. In: Nishikawa R, ed. 3rd International Workshop on Digital Mammography. Amsterdam: Elsevier 1996.
[10] Highnam RP. Model-based enhancement of mammographic images. PhD Thesis, Computing Laboratory, Oxford University, Oxford 1992.
[11] Burch A, Law J. A method for estimating compressed breast thickness during mammography. Br J Radiol 1995; 68: 394–399.
[12] Wolfe JN. Xeroradiography of the Breast. Sringfield, Il: Thomas 1972.
[13] Tabar L, Dean B. Teaching Atlas of Mammography. Stuttgart: Thieme 1983.
[14] Swann CA, Kopans DB, Koerner FC, McCarthy KA, White G, Hall DA. The halo sign and malignant breast lesions. AJR, 1987; 149: 1145–1147.
[15] Cerneaz NJ, Brady JM. Enriching digital mammogram image analysis with a description of the curvi-linear structures. In: Gale A, Astley SM, Dance DR, Cairns AY, eds. 2nd International Workshop on Digital Mammography, Excerpta Medica International Congress Series 1069, York, England. Amsterdam: Elsevier 1994: 10–12.
[16] Dance DR, Day GJ. Computation of scatter in mammography by monte carlo methods. Phys Med Biol 1984; 29: 237–247.
[17] Carlsson GA, Dance DR, Persliden J. Grids in mammography: Optimization of the information content relative to radiation risk. Technical Report ULi-RAD-R-059, Linkoping University, Department of Radiation Physics 1989.
[18] Highnam RP, Brady JM, Shepstone BJ. Removing the anti-scatter grid in mammography. In: 3rd International Workshop on Digital Mammography, Chicago, USA 1996.
[19] Shroff JH, Lloyd LR, Schroder DM. Open breast biopsy: A critical analysis. Am Surg 1991; 57(8): 481–485.
[20] Martin JE, Moskowitz M, Milbrath JR. Breast cancer missed by mammography. Am J Roentgenol 1979; 132: 737–739.
[21] Bird RE, Wallace TW, Yankaskas BC. Analysis of cancers missed at screening mammography. Radiology 1992; 184: 613–617.